We are IntechOpen, the world's leading publisher of Open Access books Built by scientists, for scientists

4,800
Open access books available

122,000
International authors and editors

135M
Downloads

154
Countries delivered to

Our authors are among the

TOP 1%
most cited scientists

12.2%
Contributors from top 500 universities

BOOK CITATION INDEX

CLARIVATE ANALYTICS

INDEXED

WEB OF SCIENCE™

Selection of our books indexed in the Book Citation Index
in Web of Science™ Core Collection (BKCI)

Interested in publishing with us?
Contact book.department@intechopen.com

Mass and Heat Transfer During Two-Phase Flow in Porous Media - Theory and Modeling

Jennifer Niessner[1] and S. Majid Hassanizadeh[2]
[1]*Institute of Hydraulic Engineering, University of Stuttgart, Stuttgart*
[2]*Department of Earth Sciences, Faculty of Geosciences, Utrecht University, Utrecht*
[1]*Germany*
[2]*The Netherlands*

1. Introduction

1.1 Motivation

This chapter focusses on the description and modeling of mass transfer processes occurring between two fluid phases in a porous medium. The principle underlying physical process comprises a transport of particles from one phase to the other phase. This process takes place across fluid–fluid interfaces (see Fig. 1) and may constitute evaporation, dissolution, or condensation, for example.

Such mass transfer processes are crucial in many applications involving flow and transport in porous media. Major examples are found in soil science (where the evaporation from soils is of interest), soil and groundwater remediation (like thermally-enhanced soil vapor extraction where dissolution, evaporation, and condensation play a role), storage of carbon dioxide in the subsurface (where the dissolution of carbon dioxide in the surrounding groundwater is a crucial storage mechanism), CO_2-enhanced oil recovery (where after primary and secondary recovery, carbon dioxide is injected into the reservoir in order to mobilize an additional 8-20 per cent of oil), and various industrial porous systems (such as certain types of fuel cells).

Let us have a closer look at a few of these applications and identify where interphase mass transfer is relevant. Four specific examples are shown in Fig. 2 and briefly described.
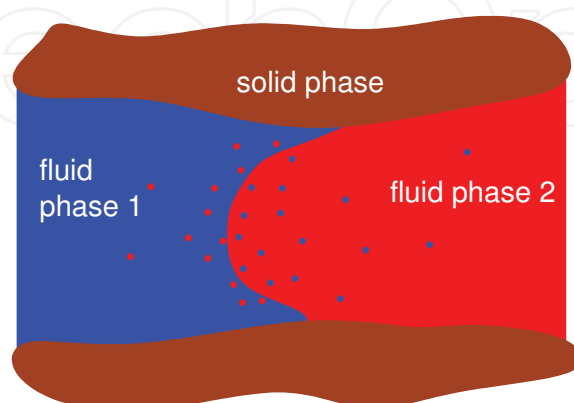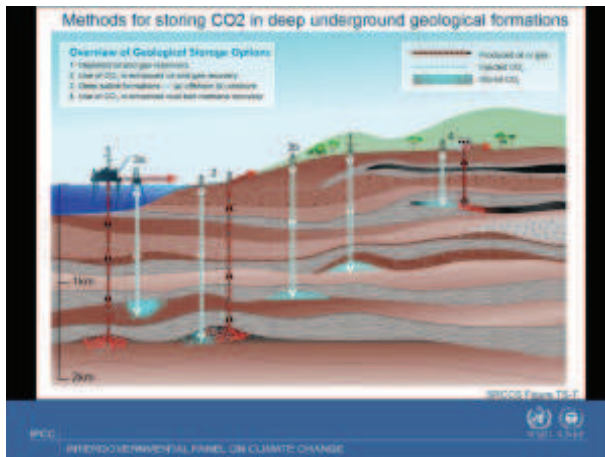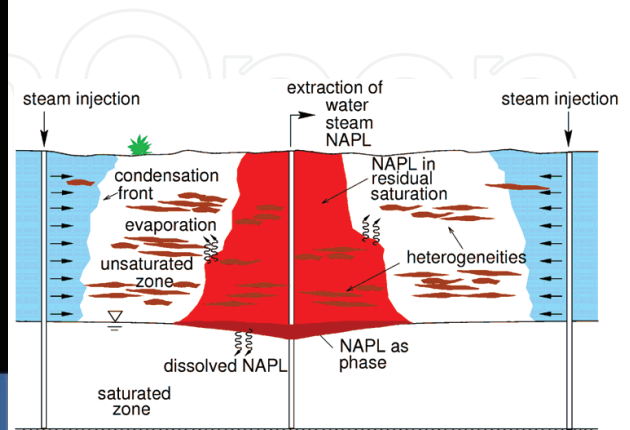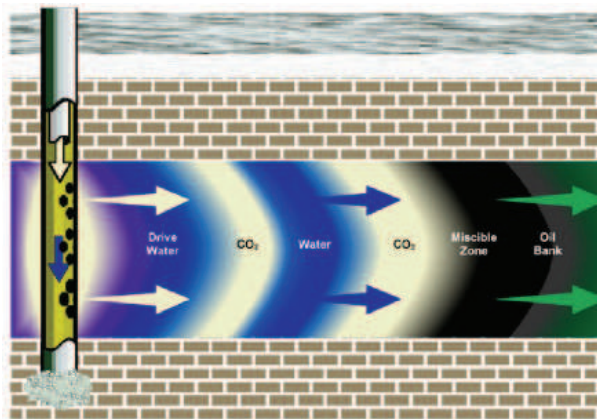

Fig. 1. Mass transfer processes (evaporation, dissolution, condensation) imply a transfer of particles across fluid–fluid interfaces.
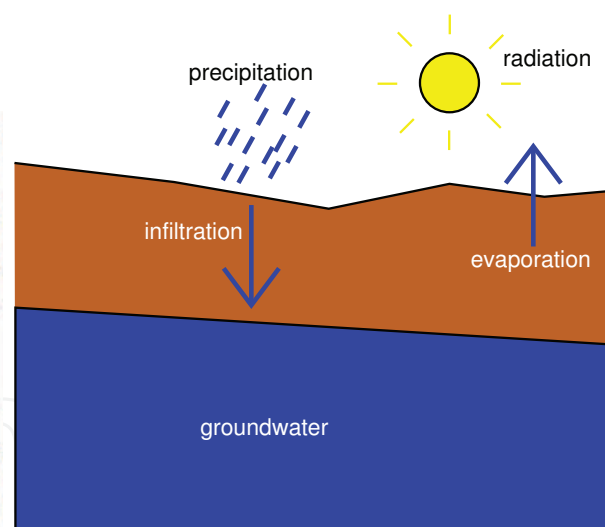
(a) Carbon dioxide storage in the subsurface (figure from IPCC (2005))

(b) Soil contamination and remediation

(c) Enhanced oil recovery (figure from www.oxy.com)

(d) Evaporation from soil

Fig. 2. Four applications of flow and transport in porous media where interphase mass transfer is important

(a) **Carbon capture and storage** (Fig. 2 (a)) is a recent strategy to mitigate the greenhouse effect by capturing the greenhouse gas carbon dioxide that is emitted e.g. by coal power plants and inject it directly into the subsurface below an impermeable caprock. Here, three different storage mechanisms are relevant on different time scales: 1) The capillary barrier mechanism of the caprock. This geologic layer is meant to keep the carbon dioxide in the storage reservoir as a separate phase. 2) Dissolution of the carbon dioxide in the surrounding brine (salty groundwater). This is a longterm storage mechanism and involves a mass transfer process as carbon dioxide molecules are "transferred" from the gaseous phase to the brine phase. 3) Geochemical reactions which immobilize the carbon dioxide through incorporation into the rock matrix.

(b) Shown in Fig. 2 (b) is a cartoon of a light **non-aqueous phase liquid (LNAPL) soil contamination** and its clean up by injection of steam at wells located around the contaminated soil. The idea behind this strategy is to mobilize the initially immobile (residual) LNAPL by evaporation of LNAPL component at large rates into the gaseous phase. The soil gas is then extracted by a centrally located extraction well. It means that the remediation mechanism relies on the evaporation of LNAPL component which represents a mass transfer from the liquid LNAPL phase into the gaseous phase.

(c) In order to produce an additional 8-20% of oil after primary and secondary recovery, carbon dioxide may be injected into an oil reservoir, e.g. alternatingly with water, see Fig. 2 (c). This is called **enhanced oil recovery**. The advantage of injecting carbon dioxide lies in the fact that it dissolves in the oil which in turn reduces the oil viscosity, and thus, increases its mobility. The improved mobility of the oil allows for an extraction of the otherwise trapped oil. Here, an interphase mass transfer process (dissolution) is responsible for an improved recovery.

(d) The last example (Fig. 2 (d)) shows the upper part of the soil. The water balance of this part of the subsurface is extremely important for agriculture or plant growth in general. Plants do not grow well under too wet or too dry conditions. One of the very important factors influencing this water balance (besides surface runoff and infiltration) is the **evaporation of water from the soil**, which is again an interphase mass transfer process.

1.2 Purpose of this work

Mass transfer processes are essential in a large variety of applications—the presented examples only show a small selection of systems. A common feature of all these applications is the fact that the relevant processes occur in relatively large domains such that it is not possible to resolve the pore structure and the fluid distribution in detail (left hand side of Fig. 3). Instead, a macro-scale approach is needed where properties and processes are averaged over a so-called representative elementary volume (right hand side of Fig. 3). This means that the common challenge in all of the above-mentioned applications is how to describe mass transfer processes on a macro scale. This transition from the pore scale to the macro scale is illustrated in Fig. 3 where on the left side, the pore-scale situation is shown (which is impossible to be resolved in detail) while on the right hand side, the macro-scale situation is shown.

2. Overview of classical mass transfer descriptions

2.1 Pore-scale considerations

In order to better understand the physics of interphase mass transfer, which is essential to provide a physically-based description of this process, we start our considerations on the pore
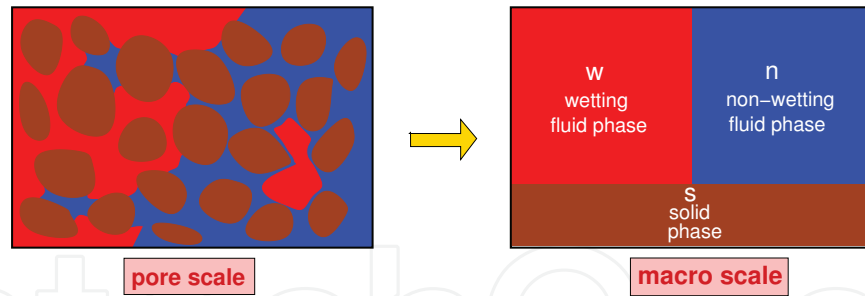
Fig. 3. Pore-scale versus macro-scale description of flow and transport in a porous medium.

scale. From there, we try to get a better understanding of the macro-scale physics of mass transfer, which is our scale of interest.

In Fig. 1 we have seen that interphase mass transfer is inherently a pore-scale process as it—naturally—takes place across fluid–fluid interfaces. Let us imagine a situation where two fluid phases, a wetting phase and a non-wetting phase, are brought in contact as shown in Fig. 4. Commonly, when the two phases are brought in contact (time $t = t_0$), equilibrium is quickly established directly at the interface. With respect to mass transfer, this means that the concentration of non-wetting phase particles in the wetting phase at the interface as well as the concentration of wetting-phase particles in the non-wetting phase at the interface are both at their equilibrium values, $C^2_{1,eq}$ and $C^1_{2,eq}$. At $t = t_0$, away from the interface, there is still no presence of α-phase particles in the β-phase. At a later time $t = t_1$, concentration profiles develop within the phases. However, within the bulk phases, the concentrations are still different from the respective equilibrium concentration at the interface. Considering a still later point of time, $t = t_2$, the equilibrium concentration is finally reached everywhere in the bulk phases.

These considerations show that mass transfer on the pore scale is inherently a kinetic process that is very much related to phase-interfaces. But how is this process represented on the macro scale, i.e. on a volume-averaged scale? This is what we will focus on in the next section.
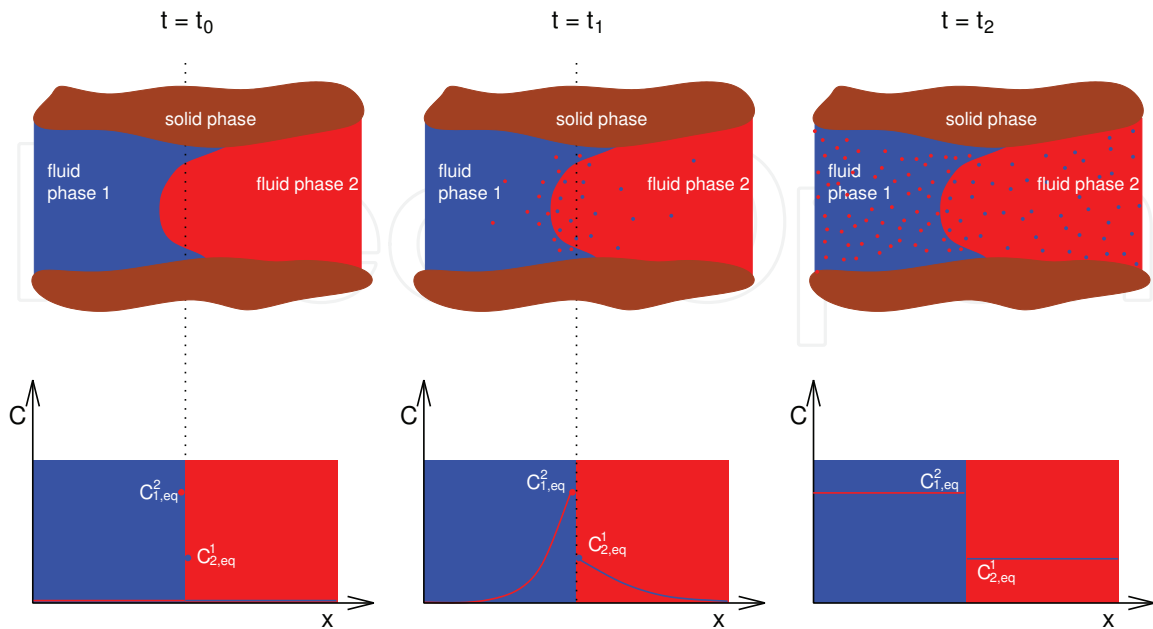

Fig. 4. Pore-scale picture of interphase mass transfer.

2.2 Current macro-scale descriptions

In Fig. 3, we illustrated the fact that when going from the pore scale to the macro scale, information about phase-interfaces is lost. The only information present on the macro scale is related to volume ratios, such as porosity and fluid saturations. But, as mentioned earlier, mass transfer is strongly linked to the presence of interfaces and interfacial areas and all the information about phase-interfaces disappears on the macro scale. This means that the description of mass transfer on the macro scale is not straight forward. Classical approaches for describing mass transfer generally rely on one of the following two principles:

1. assumption of local chemical equilibrium within an averaging volume or

2. kinetic description based on a fitted (linear) relationship.

These two classical approaches will be discussed in more detail in the following. An alternative approach which accounts for the phase-interfacial area will be presented later in Sec. 3.

2.2.1 Local equilibrium assumption

The assumption of local chemical equilibrium within an averaging volume means that the equilibrium concentrations are reached instantaneously everywhere within an averaging volume (in both phases). That means it is assumed that everywhere within the averaging volume, the situation at $t = t_2$ in Fig. 4 is reached from the beginning ($t = t_0$). Thus, at each point in the wetting phase and at each point in the non-wetting phase within the averaging volume, the equilibrium concentration of the components of the other phase is reached. This is an assumption which may be good in case of fast mass transfer, but bad in case of slow mass transfer processes. To be more precise, the assumption that the composition of a phase is at or close to equilibrium may be good if the characteristic time of mass transfer is small compared to that of flow. However, if large flow velocities occur as e.g. during air sparging, the local equilibrium assumption gives completely wrong results, see Falta (2000; 2003) and van Antwerp et al. (2008). We will investigate and quantify this issue later in Sec. 3.3 .

Local equilibrium models for multi-phase systems have been introduced and developed e.g. by Miller et al. (1990); Powers et al. (1992; 1994); Imhoff et al. (1994); Zhang & Schwartz (2000) and have been used and advanced ever since. Let us consider a system with a liquid phase (denoted by subscript l) and a gaseous phase (denoted by subscript g) composed of air and water components. Then, Henry's Law is employed to determine the mole fraction of air in the liquid phase, while the mole fraction of water in the gas phase is determined by assuming that the vapor pressure in the gas phase is equal to the saturation vapor pressure. Denoting the water component by superscript w and the air component by superscript a, this yields

$$x_l^a = p_g^a \cdot H_{l-g}^a \tag{1}$$

$$x_g^w = \frac{p_{sat}^w}{p_g}, \tag{2}$$

where $x_l^a \; [-]$ is the mole fraction of air in the liquid phase, $x_g^w \; [-]$ is the mole fraction of water in the gaseous phase, $H_{l-g}^a \; \left[\frac{1}{Pa}\right]$ is the Henry constant for the dissolution of air in the liquid phase, $p_{sat}^w \; [Pa]$ is the saturation vapor pressure of water, $p_g^a \; [Pa]$ is the partial pressure of air

in the gas phase while $p_g \, [Pa]$ is the gas pressure. The remaining mole fractions result simply from the condition that mole fractions in each phase have to sum up to one,

$$x_l^w \;=\; 1 - x_l^a \tag{3}$$
$$x_g^a \;=\; 1 - x_g^w. \tag{4}$$

Note that while for a number of applications the equilibrium mole fractions are constants or merely a function of temperature, in our case, they will be functions of space and time as pressure and the composition of the phases changes.

2.2.2 Classical kinetic approach

Kinetic mass transfer approaches are traditionally applied to the dissolution of contaminants in the subsurface which form a separate phase from water, the so-called non-aqueous phase liquids (NAPLs). If such a non-aqueous phase liquid is heavier than water, it is called "dense non-aqueous phase liquid" or DNAPL. When an immobile lense of DNAPL is present at residual saturation (i.e. at a saturation which is so low that the phase is immobile) and dissolves into the surrounding groundwater, the kinetics of this mass transfer process usually plays an important role: the dissolution of DNAPL is a rate-limited process. This is also the case when a pool of DNAPL is formed on an impermeable layer. In these relatively simple cases, only the mass transfer of a DNAPL component from the DNAPL phase into the water phase has to be considered. For these cases, classical models acknowledge the fact that the rate of mass transfer is highly dependent (proportional to) interfacial area and assume a first-order rate of kinetic mass transfer between fluid phases in a porous medium on a macroscopic (i.e. volume-averaged) scale which can be expressed as (see e.g. Mayer & Hassanizadeh (2005)):

$$Q_{\alpha \to \beta}^{\kappa} = k_{\alpha \to \beta}^{\kappa} a_{\alpha\beta}(C_{\beta,s}^{\kappa} - C_{\beta}^{\kappa}), \tag{5}$$

where $Q_{\alpha \to \beta}^{\kappa} \, \left[\frac{kg}{m^3 s}\right]$ is the interphase mass transfer rate of component κ from phase α to phase β, $k_{\alpha \to \beta}^{\kappa} \, \left[\frac{m}{s}\right]$ is the mass transfer rate coefficient, $a_{\alpha\beta} \, \left[\frac{1}{m}\right]$ is the specific interfacial area separating phases α and β, $C_{\beta,s}^{\kappa} \, \left[\frac{kg}{m^3}\right]$ is the solubility limit of component κ in phase β, and finally, $C_{\beta}^{\kappa} \, \left[\frac{kg}{m^3}\right]$ is the actual concentration of component κ in phase β. The actual concentration is not larger than the solubility limit, $C_{\beta}^{\kappa} \leq C_{\beta,s}^{\kappa}$. The case $C_{\beta}^{\kappa} = C_{\beta,s}^{\kappa}$ corresponds to the local equilibrium case.

In the absence of a physically-based estimate of interfacial area in classical kinetic models, the mass transfer coefficient $k_{\alpha \to \beta}^{\kappa}$ and the specific interfacial area $a_{\alpha\beta}$ are often lumped into one single parameter (Miller et al. (1990); Powers et al. (1992; 1994); Imhoff et al. (1994); Zhang & Schwartz (2000)). This yields, in a simplified notation,

$$Q = k(C_s - C). \tag{6}$$

Here, C_s is the solubility limit of the DNAPL component in water and C is its actual concentration. The lumped mass transfer coefficient $k \, \left[\frac{1}{s}\right]$ is commonly related to a modified Sherwood number Sh by

$$k = Sh \frac{D_m}{d_{50}^2}, \tag{7}$$

where D_m $\left[\frac{m^2}{s}\right]$ is the aqueous phase molecular diffusion coefficient, and d_{50} $[m]$ is the mean size of the grains. The Sherwood number is then related to Reynold's number Re and DNAPL saturation S_n $[-]$ by

$$Sh = pRe^q S_n^r,\tag{8}$$

where p, q, and r are dimensionless fitting parameters. This is a purely empirical relationship. Although interphase mass transfer is proportional to specific interfacial area in the original Eq. (5), this dependence cannot explicitly be accounted for as the magnitude of specific interfacial area is not known.

An alternative classical approach for DNAPL pool dissolution has been proposed by Falta (2003) who modeled the dissolution of DNAPL component by a dual domain approach for a case with simple geometry. For this purpose, they divided the contaminated porous medium into two parts: one that contains DNAPL pools and one without DNAPL. For their simple case, the dual domain approach combined with an analytical solution for steady-state advection and dispersion provided a means for modeling rate-limited interphase mass transfer. While this approach provided good results for the case of simplified geometry, it might be oversimplified for the modeling of realistic situations.

3. Interfacial-area-based approach for mass transfer description

3.1 Theoretical background

Due to a number of deficiencies of the classical model for two-phase flow in porous media (one of which is the problem in describing kinetic interphase mass transfer on the macro scale), several approaches have been developed to describe two-phase flow in an alternative and thermodynamically-based way. Among these are a rational thermodynamics approach by Hassanizadeh & Gray (1980; 1990; 1993b;a), a thermodynamically constrained averaging theory approach by Gray and Miller (e.g. Gray & Miller (2005); Jackson et al. (2009)), mixture theory (Bowen (1982)) and an approach based on averaging and non-equilibrium thermodynamics by Marle (1981) and Kalaydjian (1987). While Marle (1981) and Kalaydjian (1987) developed their set of constitutive relationships phenomenologically, Hassanizadeh & Gray (1990; 1993b); Jackson et al. (2009), and Bowen (1982) exploited the entropy inequality to obtain constitutive relationships. To the best of our knowledge, the two-phase flow models of Marle (1981); Kalaydjian (1987); Hassanizadeh & Gray (1990; 1993b); Jackson et al. (2009) are the only ones to include interfaces explicitly in their formulation allowing to describe hysteresis as well as kinetic interphase mass and energy transfer in a physically-based way. In the following, we follow the approach of Hassanizadeh & Gray (1990; 1993b) as it includes the spatial and temporal evolution of phase-interfacial areas as parameters which allows us to model kinetic interphase mass transfer in a much more physically-based way than is classically done.

It has been conjectured by Hassanizadeh & Gray (1990; 1993b) that problems of the classical two-phase flow model, like the hysteretic behavior of the constitutive relationship between capillary pressure and saturation, are due to the absence of interfacial areas in the theory. Hassanizadeh and Gray showed (Hassanizadeh & Gray (1990; 1993b)) that by formulating the conservation equations not only for the bulk phases, but additionally for interfaces, and by exploiting the residual entropy inequality, a relationship between capillary pressure, saturation, and specific interfacial areas (interfacial area per volume of REV) can be derived. This relationship has been determined in various experimental works (Brusseau et al. (1997); Chen & Kibbey (2006); Culligan et al. (2004); Schaefer et al. (2000); Wildenschild et al. (2002);

Chen et al. (2007)) and computational studies (pore-network models and CFD simulations on the pore scale, see Reeves & Celia (1996); Held & Celia (2001); Joekar-Niasar et al. (2008; 2009); Porter et al. (2009)). The numerical work of Porter et al. (2009) using Lattice Boltzman simulations in a glass bead porous medium and experiments of Chen et al. (2007) show that the relationship between capillary pressure, the specific fluid-fluid interfacial area, and saturation is the same for drainage and imbibition to within the measurement error. This allows for the conclusion that the inclusion of fluid–fluid interfacial area into the capillary pressure–saturation relationship makes hysteresis disappear or, at least, reduces it down to a very small value. Niessner & Hassanizadeh (2008; 2009a;b) have modeled two-phase flow—using the thermodynamically-based set of equations developed by Hassanizadeh & Gray (1990)—and showed that this interfacial-area-based model is indeed able to model hysteresis as well as kinetic interphase mass and also energy transfer in a physically-based way.

3.2 Simplified model

After having presented the general background of our interfacial-area-based model, we will now proceed by discussing the mathematical model. The complete set of balance equations based on the approach of Hassanizadeh & Gray (1990) is too large to be handled numerically. In order to do numerical modeling, simplifying assumptions need to be made. In the following, we present such a simplified equation system as was derived in Niessner & Hassanizadeh (2009a).

This set of balance equations can be described by six mass and three momentum balance equations. These numbers result from the fact that mass balances for each component of each phase and the fluid–fluid interface (that is 2×3) while momentum balances are given for the bulk phases and the interface. Governing equations were derived by Hassanizadeh & Gray (1979) and Gray & Hassanizadeh (1989; 1998) for the case of flow of two pure fluid phases with no mass transfer. Extending these equations to the case of two fluid phases, each made of two components, we obtain the following equations.

mass balance for phase components ($\kappa = w, a$):

$$\frac{\partial \left(\phi S_l \bar{\rho}_l \bar{X}_l^\kappa \right)}{\partial t} + \nabla \cdot \left(\phi S_l \bar{\rho}_l \bar{X}_l^\kappa \underline{v}_l \right) - \nabla \cdot \left(\phi S_l \vec{\underline{j}}_l^\kappa \right)$$
$$= \bar{\rho}_l Q_l^\kappa + \frac{1}{V} \int_{A_{lg}} \left[\rho_l X_l^\kappa \left(\underline{v}_{lg} - \underline{v}_l \right) + \underline{j}_l^\kappa \right] \cdot \underline{n}_{lg} \, dA \tag{9}$$

$$\frac{\partial \left(\phi S_g \bar{\rho}_g \bar{X}_g^\kappa \right)}{\partial t} + \nabla \cdot \left(\phi S_g \bar{\rho}_g \bar{X}_g^\kappa \underline{v}_g \right) - \nabla \cdot \left(\phi S_g \vec{\underline{j}}_g^\kappa \right)$$
$$= \bar{\rho}_g Q_g^\kappa + \frac{1}{V} \int_{A_{lg}} \left[\rho_g X_g^\kappa \left(\underline{v}_g - \underline{v}_{lg} \right) - \underline{j}_g^\kappa \right] \cdot \underline{n}_{lg} \, dA \tag{10}$$

mass balance for lg-interface components ($\kappa = w, a$):

$$\frac{\partial \left(\bar{\Gamma}_{lg} \bar{X}_{lg}^\kappa a_{lg} \right)}{\partial t} + \nabla \cdot \left(\bar{\Gamma}_{lg} \bar{X}_{lg}^\kappa a_{lg} \underline{v}_{lg} \right) - \nabla \cdot \left(\vec{\underline{j}}_{lg}^\kappa a_{lg} \right) -$$
$$= \frac{1}{V} \int_{A_{lg}} \left[\rho_l X_l^\kappa \left(\underline{v}_l - \underline{v}_{lg} \right) - \underline{j}_l^\kappa - \rho_g X_g^\kappa \left(\underline{v}_g - \underline{v}_{lg} \right) + \underline{j}_g^\kappa \right] \cdot \underline{n}_{lg} \, dA \tag{11}$$

momentum balance for phases:

$$\frac{\partial \left(\phi S_l \bar{\rho}_l \bar{\underline{v}}_l \right)}{\partial t} + \nabla \cdot \left(\phi S_l \bar{\rho}_l \bar{\underline{v}}_l \bar{\underline{v}}_l \right) - \nabla \cdot \left(\phi S_l \underline{T}_l \right)$$

$$= \frac{1}{V} \int_{A_{lg}} \left[\rho_l \underline{v}_l \left(\underline{v}_{lg} - \underline{v}_l \right) + \underline{t}_l \right] \cdot \underline{n}_{lg} \, dA \tag{12}$$

$$\frac{\partial \left(\phi S_g \bar{\rho}_g \bar{\underline{v}}_g \right)}{\partial t} + \nabla \cdot \left(\phi S_g \bar{\rho}_g \bar{\underline{v}}_g \bar{\underline{v}}_g \right) - \nabla \cdot \left(\phi S_g \underline{T}_g \right)$$

$$= \frac{1}{V} \int_{A_{lg}} \left[\rho_g \underline{v}_g \left(\underline{v}_g - \underline{v}_{lg} \right) - \underline{t}_g \right] \cdot \underline{n}_{lg} \, dA \tag{13}$$

momentum balance for *lg*-interface:

$$\frac{\partial \left(\bar{\Gamma}_{lg} \bar{\underline{v}}_{lg} a_{lg} \right)}{\partial t} + \nabla \cdot \left(\bar{\Gamma}_{lg} \bar{\underline{v}}_{lg} a_{lg} \bar{\underline{v}}_{lg} \right) - \nabla \cdot \left(\underline{T}_{lg} a_{lg} \right)$$

$$= \frac{1}{V} \int_{A_{lg}} \left[\rho_l \underline{v}_l \left(\underline{v}_l - \underline{v}_{lg} \right) - \underline{t}_l - \rho_g \underline{v}_g \left(\underline{v}_g - \underline{v}_{lg} \right) + \underline{t}_g \right] \cdot \underline{n}_{lg} \, dA, \tag{14}$$

where the overbars denote volume-averaged (macro-scale) quantities. Here, $X_\alpha^\kappa \ [-]$ is the mass fraction of component κ in phase α, t is time, $Q_\alpha^\kappa \ \left[\frac{m^3}{s} \right]$ is an external source of component κ in phase α, $\underline{j}_\alpha^\kappa \ \left[\frac{kg \cdot m^4}{s} \right]$ is the diffusive flux of component κ in phase α, V is the magnitude of the averaging volume, A_{lg} denotes the interfaces separating the *l*-phase and the *g*-phase in an averaging volume, $\underline{v}_{lg} \ \left[\frac{m}{s} \right]$ is the velocity of the *lg*-interface, and $\underline{n}_{lg}$ is the unit vector normal to A_{lg} and pointing into the *g*-phase. Furthermore, $X_{lg}^\kappa \ [-]$ is the mass fraction of component κ in the *lg*-interface, $\underline{j}_{lg}^\kappa \ \left[\frac{kg \cdot m^4}{s} \right]$ is the diffusive flux of component κ in the *lg*-interface, $\underline{t}_\alpha \ \left[\frac{kg}{m \cdot s^2} \right]$ is the α-phase micro-scale stress tensor, $\underline{T}_\alpha \ \left[\frac{kg}{s^2} \right]$ is the α-phase macro-scale stress tensor, and $\underline{T}_{lg} \ \left[\frac{kg}{s^2} \right]$ is the macro-scale *lg*-interfacial stress tensor.

In the following, we provide a simplified version of Eq. (9) through (14). First, we assume that the composition of the interface does not change. This is a reasonable assumption as long as no surfactants are involved. This reduces the number of balance equations to eight, as we can sum up the mass balance equations for interface components. Furthermore, we assume that momentum balances can be simplified so far that we end up with Darcy-like equations for both bulk phases and interface. We further proceed by applying Fick's law to relate the micro-scale diffusive fluxes $\underline{j}_\alpha^\kappa$ to the local concentration gradient resulting in the following approximation:

$$\underline{j}_\alpha^\kappa \cdot \underline{n}_{lg} = \pm \frac{\rho_\alpha D^\kappa}{d^\kappa} a_{lg} \left(X_{\alpha,s}^\kappa - X_\alpha^\kappa \right), \tag{15}$$

where $D^\kappa \ \left[\frac{m^2}{s} \right]$ is the micro-scale Fickian diffusion coefficient for component κ, $d^\kappa \ [m]$ is the diffusion length of component κ, $X_{\alpha,s}^\kappa \ [-]$ is the solubility limit of component κ in phase α (i.e. the mass fraction corresponding to local equilibrium), and $X_\alpha^\kappa \ [-]$ is the micro-scale mass fraction of component κ in phase α at a distance d^κ away from the interface. Niessner &

Hassanizadeh (2009a) obtained the following determinate set of macro-scale equations:

$$\frac{\partial \left(\phi S_l \bar{\rho}_l \bar{X}_l^w \right)}{\partial t} \quad + \quad \nabla \cdot \left(\bar{\rho}_l \bar{X}_l^w \underline{\bar{v}}_l \right) - \nabla \cdot \left(\underline{\vec{j}}_l^w \right)$$
$$= \quad \rho_l Q_l^w - \frac{D^w \bar{\rho}_g}{d^w} a_{lg} \left(X_{g,s}^w - X_g^w \right) \tag{16}$$

$$\frac{\partial \left(\phi S_l \bar{\rho}_l \bar{X}_l^a \right)}{\partial t} \quad + \quad \nabla \cdot \left(\bar{\rho}_l \bar{X}_l^a \underline{\bar{v}}_l \right) - \nabla \cdot \left(\underline{\vec{j}}_l^a \right)$$
$$= \quad \rho_l Q_l^a + \frac{D^a \bar{\rho}_l}{d^a} a_{lg} \left(X_{l,s}^a - X_l^a \right) \tag{17}$$

$$\frac{\partial \left(\phi S_g \bar{\rho}_g \bar{X}_g^w \right)}{\partial t} \quad + \quad \nabla \cdot \left(\bar{\rho}_g \bar{X}_g^w \underline{\bar{v}}_g \right) - \nabla \cdot \left(\underline{\vec{j}}_g^w \right)$$
$$= \quad \rho_g Q_g^w + \frac{D^w \bar{\rho}_g}{d^w} a_{lg} \left(X_{g,s}^w - X_g^w \right) \tag{18}$$

$$\frac{\partial \left(\phi S_g \bar{\rho}_g \bar{X}_g^a \right)}{\partial t} \quad + \quad \nabla \cdot \left(\bar{\rho}_g \bar{X}_g^a \underline{\bar{v}}_g \right) - \nabla \cdot \left(\underline{\vec{j}}_g^a \right)$$
$$= \quad \rho_g Q_g^a - \frac{D^a \bar{\rho}_l}{d^a} a_{lg} \left(X_{l,s}^a - X_l^a \right) \tag{19}$$

$$\frac{\partial a_{lg}}{\partial t} + \nabla \cdot \left(a_{lg} \underline{v}_{lg} \right) \quad = \quad E_{lg} \tag{20}$$

$$\underline{\bar{v}}_l \quad = \quad -K \frac{S_l^2}{\mu_l} \left(\nabla p_l - \bar{\rho}_l \underline{g} \right) \tag{21}$$

$$\underline{\bar{v}}_g \quad = \quad -K \frac{S_g^2}{\mu_g} \left(\nabla p_g - \bar{\rho}_g \underline{g} \right) \tag{22}$$

$$\underline{\bar{v}}_{lg} \quad = \quad -K_{lg} \nabla a_{lg} \tag{23}$$

$$p_c \quad = \quad p_g - p_l \tag{24}$$

$$S_l + S_g \quad = \quad 1 \tag{25}$$

$$X_l^w + X_l^a \quad = \quad 1 \tag{26}$$

$$X_g^w + X_g^a \quad = \quad 1 \tag{27}$$

$$a_{lg} \quad = \quad a_{lg}(S_l, p_c), \tag{28}$$

The macro-scale mass fluxes $\underline{\vec{j}}_\alpha^\kappa$ are given by a Fickian dispersion equation,

$$\underline{\vec{j}}_\alpha^\kappa = -\rho_\alpha \bar{D}_\alpha^\kappa \nabla \left(\bar{X}_\alpha^\kappa \right), \tag{29}$$

where $\bar{D}_\alpha^\kappa$ is the macro-scale dispersion coefficient. Note that in Eq. (16) through (19), we have acknowledged the fact that an internal source of a component in one of the phases must correspond to a sink of that component of equal magnitude in the other phase. The solubility limits $X_{g,s}^w$ and $X_{l,s}^a$ are obtained from a local equilibrium assumption at the fluid–fluid interface. If, for example, we consider a two-phase–two-component air–water system solubility limits with respect to mole fractions are given by Eqs. (1) and (2).

3.3 Is a kinetic approach necessary?

Depending on the parameters, initial conditions, and boundary conditions of the system, kinetics might be important for mass transfer. If so, then it may not be sufficient to use a classical local equilibrium model instead of the more complex interfacial-area-based model. To allow for a decision, Niessner & Hassanizadeh (2009a) make the system of equations (16) through (28) dimensionless and study the dependence of kinetics on Damköhler number and Peclet number.

To do so, they define dimensionless variables:

$$t^* = \frac{t v_R}{\phi L}, \qquad \nabla^* = L\nabla, \qquad \bar{v}_\alpha^* = \frac{\bar{v}_\alpha}{v_R}, \qquad Q_\alpha^{\kappa*} = \frac{Q_\alpha^\kappa L}{X_{\alpha,s}^\kappa v_R}, \tag{30}$$

$$a_{lg}^* = \frac{a_{lg}}{a_{R,lg}}, \qquad \bar{D}_\alpha^{\kappa*} = \frac{\bar{D}_\alpha^\kappa}{D_{R,\alpha}}, \qquad v_{lg}^* = \frac{\phi}{v_R} v_{lg}, \tag{31}$$

$$E_{lg}^* = \frac{a_{R,lg}\phi L}{v_R} E_{lg}, \qquad \underline{g}_\alpha^* = \frac{\bar{\rho}_\alpha \underline{g} L}{p_R}, \qquad K_{lg}^* = \frac{\phi K_{lg}}{L a_{R,lg} v_R}, \tag{32}$$

$$p_\alpha^* = \frac{p_\alpha}{p_R}, \qquad p_c^* = \frac{p_c}{p_R}, \qquad \rho_g^* = \frac{\bar{\rho}_g}{\bar{\rho}_l} \qquad \mu_l^* = \frac{\mu_l}{\mu_g}. \tag{33}$$

Here, ρ_g^* is density ratio, μ_l^* is viscosity ratio, v_R is a reference velocity, L is a characteristic length, $a_{R,lg}$ is a reference specific interfacial area, $D_{R,\alpha}$ is a reference dispersion coefficient, and p_R is a reference pressure. We assume that p_R and v_R can be chosen such that $\frac{K p_R}{\mu_l v_R L} = 1$. Also, Peclet number Pe_α and Damköhler number Da^κ are defined by

$$\text{Pe}_\alpha = \frac{v_R L}{D_{R,\alpha}}, \qquad \text{Da}^\kappa = \frac{D^\kappa L a_{R,lg}}{d v_R}. \tag{34}$$

These definitions lead to the following dimensionless form of Eq. (16) through (28):

$$\frac{\partial}{\partial t^*}\left(S_l \bar{X}_l^w\right) + \nabla^* \cdot \left(\bar{X}_l^w \underline{v}_l^*\right) - \nabla^* \cdot \left(\frac{D_l^{w*}}{\text{Pe}_l}\nabla^* \bar{X}_l^w\right) = Q_l^{w*} - \text{Da}^w a_{lg}^* \rho_g^*\left(X_{g,s}^w - \bar{X}_g^w\right) \tag{35}$$

$$\frac{\partial}{\partial t^*}\left(S_l \bar{X}_l^a\right) + \nabla^* \cdot \left(\bar{X}_l^a \underline{v}_l^*\right) - \nabla^* \cdot \left(\frac{D_l^{a*}}{\text{Pe}_l}\nabla^* \bar{X}_l^a\right) = Q_l^{a*} + \text{Da}^a a_{lg}^*\left(X_{l,s}^a - \bar{X}_l^a\right) \tag{36}$$

$$\frac{\partial}{\partial t^*}\left(S_g \bar{X}_g^w\right) + \nabla^* \cdot \left(\bar{X}_g^w \underline{v}_g^*\right) - \nabla^* \cdot \left(\frac{D_g^{w*}}{\text{Pe}_g}\nabla^* \bar{X}_g^w\right) = Q_g^{w*} + \text{Da}^w a_{lg}^*\left(X_{g,s}^w - \bar{X}_g^w\right) \tag{37}$$

$$\frac{\partial}{\partial t^*}\left(S_g \bar{X}_g^a\right) + \nabla^* \cdot \left(\bar{X}_g^a \underline{v}_g^*\right) - \nabla^* \cdot \left(\frac{D_g^{a*}}{\text{Pe}_g}\nabla^* \bar{X}_g^a\right) = Q_g^{a*} - \text{Da}^a a_{lg}^* \frac{1}{\rho_g^*}\left(X_{l,s}^a - \bar{X}_l^a\right) \tag{38}$$

$$\frac{\partial a_{lg}^*}{\partial t^*} + \nabla^* \cdot \left(a_{lg}^* \underline{v}_{lg}^*\right) = E_{lg}^* \tag{39}$$

$$\underline{v}_l^* = -S_l^2\left(\nabla^* p_l^* - \underline{g}_l^*\right) \tag{40}$$

$$\underline{v}_g^* = -S_g^2 \mu_l^*\left(\nabla^* p_g^* - \underline{g}_g^*\right) \tag{41}$$

$$\underline{v}_{lg}^* = -K_{lg}^* \nabla^* a_{lg}^* \tag{42}$$

$$p_c^* = p_g^* - p_l^* \tag{43}$$

$$S_l + S_g = 1 \tag{44}$$

$$\bar{X}_l^w + \bar{X}_l^a = 1 \tag{45}$$

$$\bar{X}_g^w + \bar{X}_g^a = 1 \tag{46}$$

$$a_{lg}^* = a_{lg}^* (S_l, p_c^*). \tag{47}$$

In order to investigate the importance of kinetics, we define $\mathrm{Pe} := \mathrm{Pe}_l = \mathrm{Pe}_g$ and $\mathrm{Da} := \mathrm{Da}^w = \mathrm{Da}^a$ and vary Pe and Da independently over five orders of magnitude. Therefore, we consider a numerical example where dry air is injected into a horizontal (two-dimensional) porous medium of size 0.7 m × 0.5 m that is almost saturated with water (initial and boundary water saturation of 0.9).

Fig. 5 shows a comparison of actual mass fractions $\bar{X}_l^a$ and $\bar{X}_g^w$ to solubility mass fractions $X_{l,s}^a$ and $X_{g,s}^w$ for five different Damköhler numbers. Therefore, a cut through the domain is shown and two different time steps are compared.
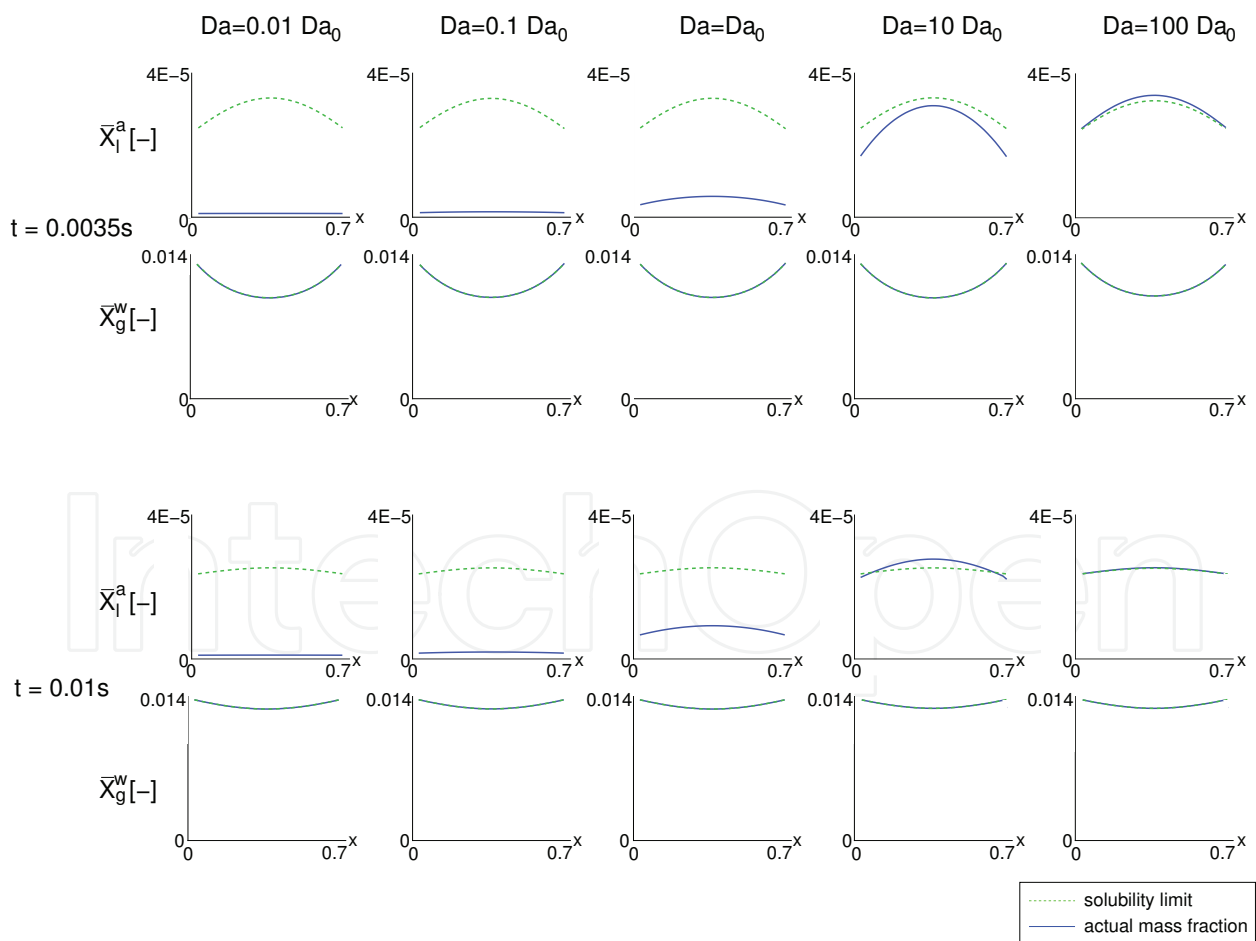
Fig. 5. Solubility limits $X_{l,s}^a$ and $X_{g,s}^w$ and actual mass fractions $\bar{X}_l^a$ and $\bar{X}_g^w$ for two different time steps (0.0035 s and 0.01 s) and 5 different Damköhler numbers.

It can be seen that the system is practically instantaneously in equilibrium with respect to the mass fraction $\bar{X}_g^w$ (water mass fraction in the gas phase) for the whole range of considered Damköhler numbers (see the second and forth row of graphs). With respect to the mass fraction $\bar{X}_l^a$ (air mass fraction in the water phase), for low Damköhler numbers and early times, the system is far from equilibrium (see the first and third row of graphs). With increasing time and with increasing Damköhler number, the system approaches equilibrium. As for high Damköhler numbers mass transfer is very fast, an "overshoot" occurs and the system becomes oversaturated before it reaches equilibrium.

One might argue that the considered time steps are extremely small and not relevant for the time scale relevant for the whole domain. However, what happens at this very early time has a large influence on the state of the system at all subsequent times.

It turned out that for different Peclet numbers, there is no difference in results. That means that kinetic interphase mass transfer is independent of Peclet number, at least within the four orders of magnitude considered here.

4. Extension to heat transfer

The concept of describing mass transfer based on modeling the evolution of interfacial areas using the thermodynamically-based approach of Hassanizadeh & Gray (1990; 1993b) can be extended to describing interphase heat transfer as well. The main difference between interphase mass and heat transfer is that, in addition to fluid–fluid interfaces, heat can also be transferred across fluid–solid interfaces, see Fig. 6.

Similarly to mass transfer, classical two-phase flow models describe heat transfer on the macro scale by either assuming local thermal equilibrium within an averaging volume or by formulating empirical models to describe the transfer rates. The latter is necessary as classically, both fluid–fluid and fluid–solid interfacial areas are unknown on the macro scale. And similarly to mass transfer, we can use the thermodynamically-based approach of Hassanizadeh & Gray (1990; 1993b) which includes both fluid–fluid and fluid–solid interfacial areas in order to describe mass transfer in a physically-based way. We can
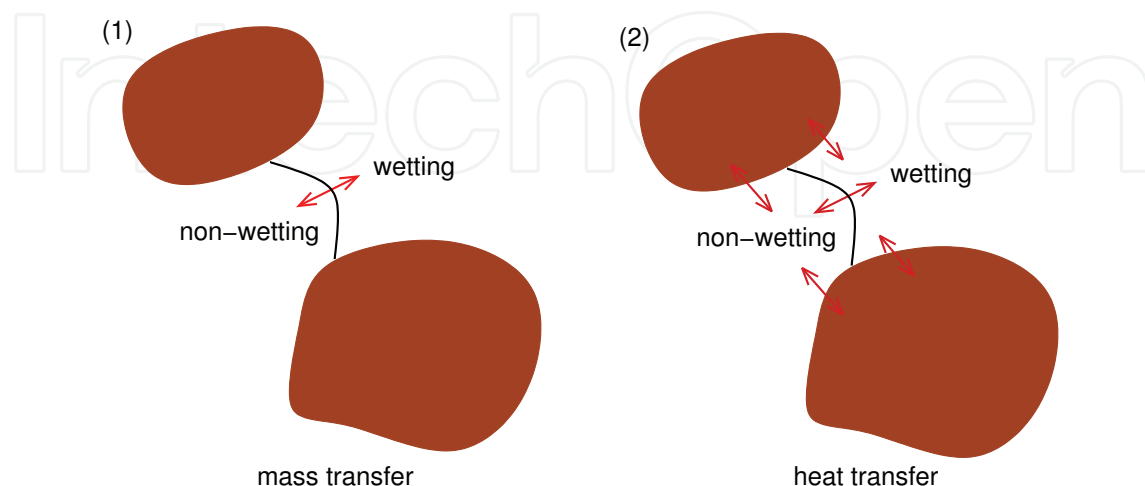

Fig. 6. Mass transfer takes place across fluid–fluid interfaces (left hand side) and heat transfer across fluid–fluid as well as fluid–solid interfaces (right hand side)

also perform a dimensional analysis and derive dimensionless numbers that help to decide whether kinetics of heat transfer needs to be accounted for or whether a local equilibrium model is sufficiently accurate on the macro scale. For more details on these issues, we refer to Niessner & Hassanizadeh (2009b).

5. Macro-scale example simulations

For the numerical solution of the system of Eq.s (16) through (28), we use a fully-coupled vertex-centered finite element method (an in-house code) which not only conserves mass locally, but is also applicable to unstructured grids. For time discretization, a fully implicit Eulerian approach is used, see e.g. Bastian et al. (1997); Bastian & Helmig (1999). The nonlinear system is linearized using a damped inexact Newton-Raphson solver, and the linear system is subsequently solved using a Bi-Conjugate Gradient Stabilized method (known as BiCGStab method). Full upwinding is applied to the flux terms of the bulk phase equations, but in the interfacial area flux term, central weighting is used.

5.1 Evaporator

As a simulation example, we consider a setup which is relevant in many industrial processes where a product needs to be concentrated (e.g. foods, chemicals, and salvage solvents) or dried through evaporation of water. The aqueous solution containing the desired product is fed into the evaporator mostly consisting of micro-channels and then passes a heat source. Heat converts the water in the solution into vapor and the vapor is subsequently removed from the solution. We model the heating and evaporation process through a setup as shown in Fig. 7.

This means we consider a horizontal domain that is closed along the sides (top and bottom in the figure) and that is subjected to a gradient in wetting phase pressure from left to right in the undisturbed situation. This system is assumed to be at the following initial conditions: a temperature of 293 K, gas phase at atmospheric pressure, water saturation of 0.9, a corresponding capillary pressure based on the primary drainage curve, and mass fractions that correspond to the local chemical equilibrium conditions as prescribed by Henry's Law and Raoult's Law (Lüdecke & Lüdecke (2000)). The porous medium is heated with a rate of Q_s in a square-shaped part of the domain, causing the evaporation of water (see Fig. 7). Note that the heat source heats up only the walls of the microchannels (the solid phase) and the heat is then transferred from the solid phase to the water phase.
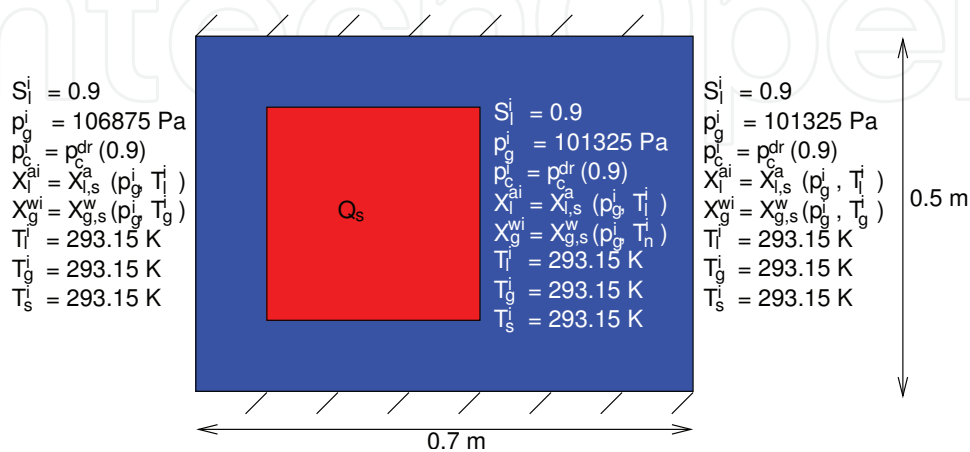

Fig. 7. Setup of the numerical example: water passes a heat source and is evaporated.

For comparison, the same setup is used for simulations using a classical two-phase flow model, where—in the absence of interfacial areas as parameters—local chemical and thermal equilibrium is assumed. This means that the heat source cannot be defined for the solid phase only; instead, the applied heat will instantaneously lead to a heating of all three phases.

The distribution of water saturation and water–gas specific interfacial area are shown in Fig. 8 at the time of 17 seconds after the heat source is switched on. The saturation distribution given by the interfacial area-based model is compared to that of the classical model. Obviously, water saturation decreases in the heated region due to the evaporation of water. Downstream of the heated zone, water saturation increases indicating that in the colder regions, water condenses again. Due to the decrease in water saturation, gas–water interfacial areas are created. The classical model predicts a much lower decrease in water saturation in the heated region.

Fig. 9 shows the mass fraction of air dissolved in the liquid phase after 17 seconds. There, also the equilibrium value (solubility limit) predicted by the interfacial area-based model is shown. Clearly, chemical non-equilibrium effects occur, but the classical model predicts approximately the same result as the equilibrium values in the interfacial area-based model. This is due to the fact that the classical two-phase flow approach always assumes local equilibrium and can only represent mass fractions corresponding to the equilibrium values.

The analogous comparison is shown in Fig. 10 with respect to the mass fractions of vapor in the gas phase.

Here, the mass fractions in the interfacial area-based model are very close to the equilibrium values, but larger differences to the classical model can be detected.
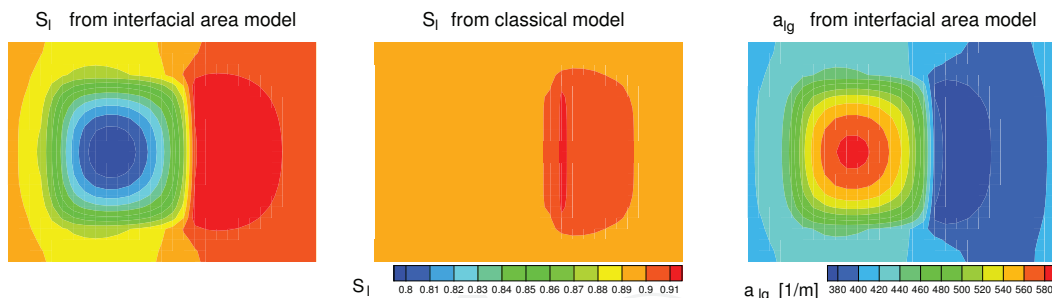
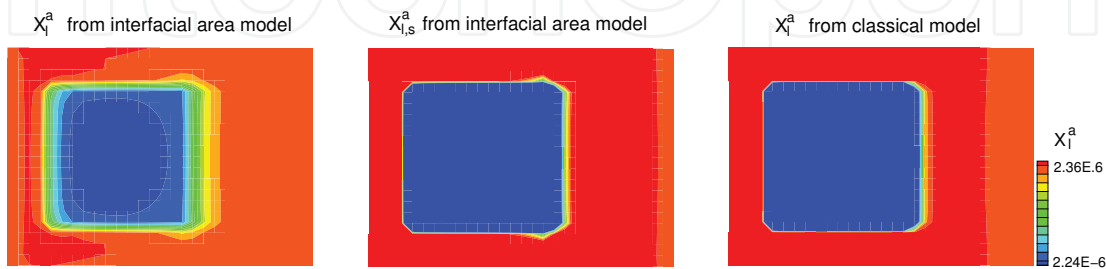Fig. 8. Water saturation and water–gas specific interfacial area after 17s.

Fig. 9. Mass fraction of air in the liquid phase after 17s. Left: results using the interfacial area-based model, middle: equilibrium values given by the interfacial area-based model, right: results given by the classical model.
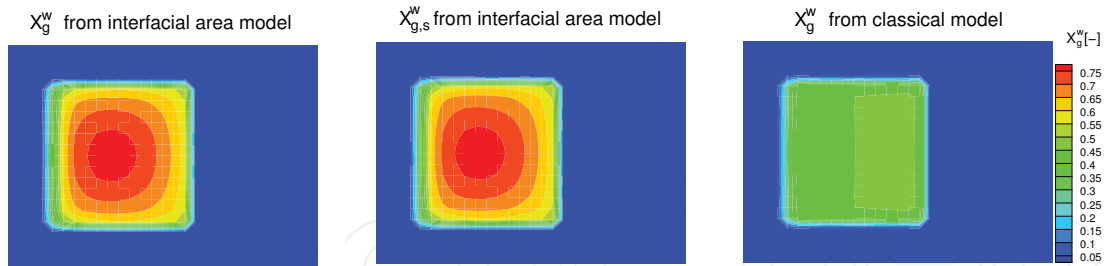
Fig. 10. Mass fractions of vapor in the gas phase after 17s. Left: results using the interfacial area-based model, middle: equilibrium values given by the interfacial area-based model, right: results given by the classical model.

Fig. 11 shows the temperatures of the three phases (liquid l, gas g, solid s) after 17s using the interfacial area-based model and the classical model. It can be seen that a lower temperature rise is predicted by the classical model than by the interfacial area-based model.
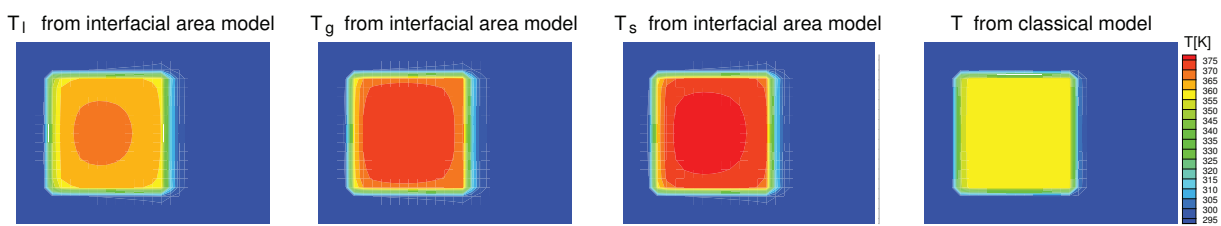
Fig. 11. Temperatures of the phases after 17s using the interfacial area-based model (three pictures on left) and the classical model (right picture).

Fig. 12 shows the temperature differences between the phases using the interfacial area-based model. We find that there are differences of up to 8 K between the phases. The classical two-phase model assumes local thermal equilibrium, i.e. $T_w = T_n = T_s$. In reality, however, the heat exchange between the phases is restricted by the respective interfacial areas and the heat equalization does not take place instantaneously.
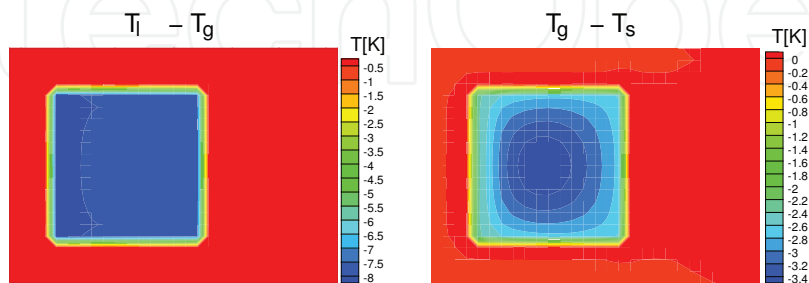
Fig. 12. Temperatures differences between wetting and non-wetting phase (left hand side) and between non-wetting and solid phase (right hand side) after 17s.

5.2 Drying of a porous medium

As a second example, we consider the drying of an initially almost water-saturated porous medium through injection of hot dry air (50 °C). This process is relevant in the textile, construction, and paper industries as well as in medical applications. The setup is shown in Fig. 13. For comparison, this setup is also simulated using the classical model. Note that in the classical model, due to the assumption of local chemical and thermal equilibrium, it is impossible to apply a source of hot dry air. Instead, the air supplied to the system instantaneously redistributes among the phases in order to yield equilibrium composition. The temperature of the air source will instantaneously heat up all three phases.
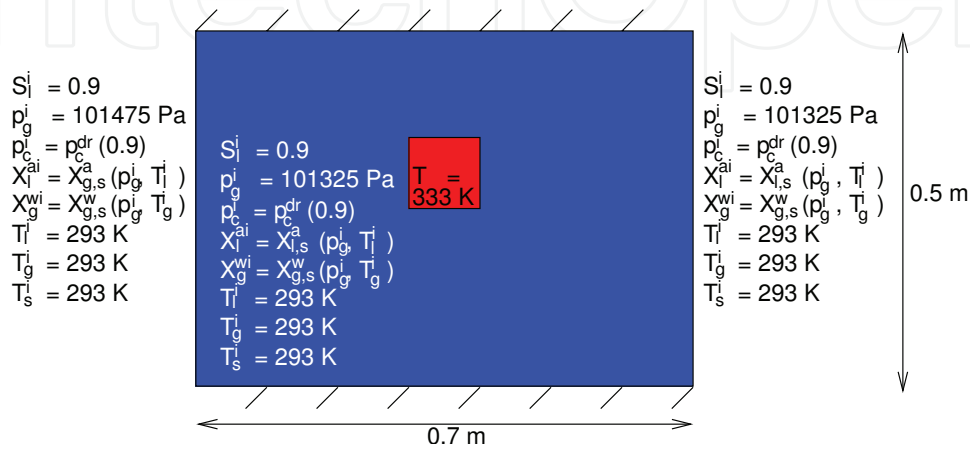
Fig. 13. Setup of the numerical example: drying of a porous medium through injection of warm dry air.

Fig. 14 shows the water saturation and the specific gas–water interfacial area after 12 seconds. The water saturation decreases due to the gas injection and interfaces are produced. The saturation distribution is different if the classical model is used. This may be due to the fact that the source term needs to be specified differently for the two models (see the above comments on the problem description).
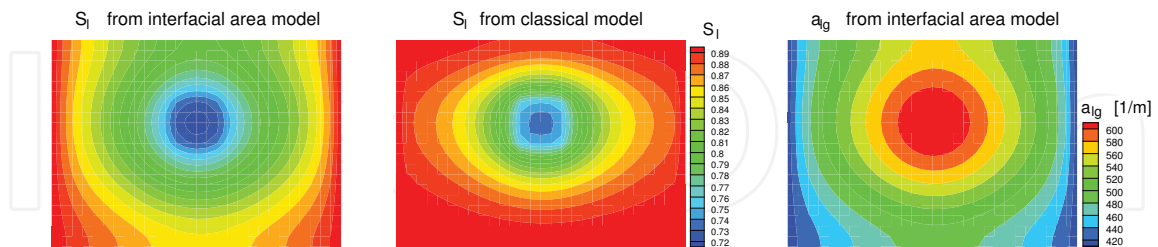

Fig. 14. Water saturation (using both interfacial area-based and classical model) and specific fluid–fluid interfacial area using the interfacial area-based model after 12s.

In Fig. 15, the mass fraction of air disolved in the water phase is shown after 12s. The actual mass fraction distribution using the interfacial-area-based approach is shown in the left picture. The mass fraction corresponding to local chemical equilibrium is shown in the middle figure. For comparison, the mass fraction distribution resulting from the classical model is shown in the right figure. Obviously, significant deviations from equilibrium can be detected. This implies that chemical non-equilibrium is very important in this example. The
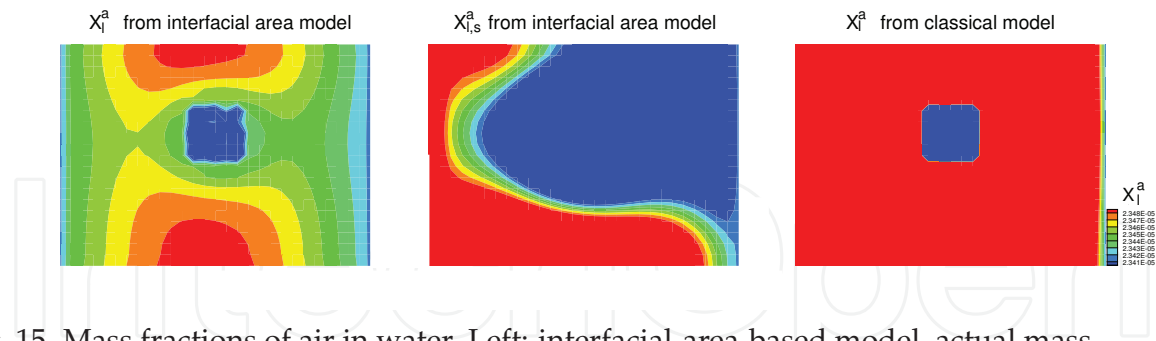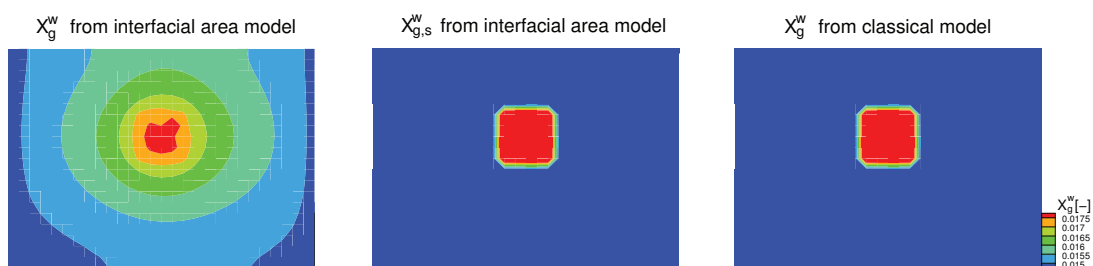
Fig. 15. Mass fractions of air in water. Left: interfacial-area-based model, actual mass fractions; middle: equilibrium mass fractions. Right: classical model.

equilibrium mass fractions of the interfacial area-based model are also very different from that predicted by the classical model, probably due to the differently specified source.

Fig. 16 shows the same for water vapor in the gas phase. Here, the deviation from chemical equilibrium is also significant, but the equilibrium mass fractions using the interfacial area-based model and the classical model are very similar.

Fig. 16. Mass fractions of vapor in the gas phase. Left: interfacial-area-based model, actual mass fractions; middle: equilibrium mass fractions. Right: classical model.

In Fig. 17, the temperatures of the three phases (liquid l, gas g, and solid phase s) resulting from the interfacial area-based model are shown and compared to the temperature given by the classical model. Unlike the mass fractions, the temperatures are not very far from equilibrium (maximum difference in phase temperatures is approximately 0.17 K, see also Fig. 18). An interesting aspect is that the temperature difference is lower in the middle of the injection zone than in the surrounding area. This is due to the fact that specific interfacial area is at a maximum in this middle part leading to higher heat transfer rates in this region and phase temperature closer to each other and thus, closer to thermal equilibrium.

6. Summary and conclusions

In this chapter, the issue of interphase mass transfer during two-phase flow in a porous medium has been discussed. Starting from pore-scale considerations, the classical approaches for describing mass transfer have been presented which—due to the absence of interfacial area as a parameter—either assume local equilibrium within an averaging volume or use empirical approaches to describe the kinetics.
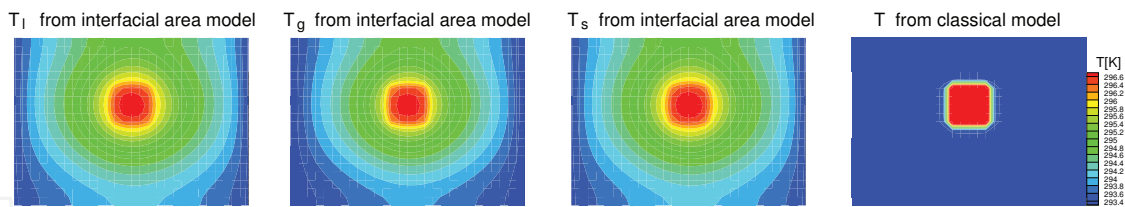
Fig. 17. Temperatures of the phases using the interfacial area-based model (three pictures on left hand side) and the classical model (right hand side picture).
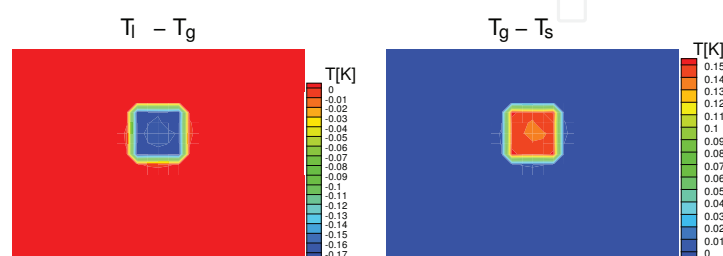

Fig. 18. Temperature differences between the phases.

As an alternative, a thermodynamically-based model was presented which explicitly accounts for the presence of interfaces and describes their evolution in space and time. Due to the knowledge of interfacial area, kinetic interface mass transfer can be modeled in a physically-based way. In order to decide whether kinetics of mass transfer needs to be accounted for or whether an equilibrium model would give sufficiently good results, a dimensional analysis was carried through. Also, the concept was extended to kinetic interphase heat transfer where in addition to fluid–fluid interfaces, fluid–solid interfaces are important. Two examples have illustrated the issues presented: in our results, we could observe that in the drying example, chemical non-equilibrium is significant. In the evaporator example, contrarily, thermal non-equilibrium is very pronounced.

In order to advance the description of real life systems, such as those described in Sec. 1.1, an important future step would be to apply the presented model concept to practical applications and to verify the results by comparison to experimental data.

7. Acknowledgements

8. References

Bastian, P., Birken, K., Johannsen, K., Lang, S., Eckstein, K., Neuss, N., Rentz-Reichert, H. & Wieners, C. (1997). UG - A Flexible Software Toolbox for Solving Partial Differential Equations, Computing and Visualization in Science, 1(1):27–40.

Bastian, P. & Helmig, R. (1999). Efficient Fully-Coupled Solution Techniques for Two Phase Flow in Porous Media. Parallel Multigrid Solution and Large Scale Computations.,

Advances in Water Resources 23: 199–216.

Bowen, R. (1982). Compressible Porous Media Models by Use of the Theory of Mixtures, *International Journal of Engineering Science* 20(6): 697–735.

Brusseau, M., Popovicova, J. & Silva, J. (1997). Characterizing gas–water interfacial and bulk-water partitioning for gas phase transport of organic contaminants in unsaturated porous media, *Environmental Sciences Technology* 31: 1645–1649.

Chen, D., Pyrak-Nolte, L., Griffin, J. & Giordano, N. (2007). Measurement of interfacial area per volume for drainage and imbibition, *Water Resources Research* 43(12).

Chen, L. & Kibbey, T. (2006). Measurement of air–water interfacial area for multiple hysteretic drainage curves in an unsaturated fine sand, *Langmuir* 22: 6674–6880.

Culligan, K., Wildenschild, D., Christensen, B., Gray, W., Rivers, M. & Tompson, A. (2004). Interfacial area measurements for unsaturated flow through a porous medium, *Water Resources Research* 40: 1–12.

Falta, R. W. (2000). Numerical modeling of kinetic interphase mass transfer during air sparging using a dual-media approach, *Water Resources Research* 36(12): 3391–3400.

Falta, R. W. (2003). Modeling sub-grid-block-scale dense nonaqueous phase liquid (DNAPL) pool dissolution using a dual-domain approach, *Water Resources Research* 39(12).

Gray, W. & Hassanizadeh, S. (1989). Averaging theorems and averaged equations for transport of interface properties in multiphase systems, *International Journal of Multi-Phase Flow* 15: 81–95.

Gray, W. & Hassanizadeh, S. (1998). Macroscale continuum mechanics for multiphase porous-media flow including phases, interfaces, common lines, and common points, *Advances in Water Resources* 21: 261–281.

Gray, W. & Miller, C. (2005). Thermodynamically Constrained Averaging Theory Approach for Modeling of Flow in Porous Media: 1. Motivation and Overview, *Advances in Water Resources* 28(2): 161–180.

Hassanizadeh, S. M. & Gray, W. G. (1979). General Conservation Equations for Multi-Phase Systems: 2. Mass, Momenta, Energy, and Entropy Equations, *Advances in Water Resources* 2: 191–203.

Hassanizadeh, S. M. & Gray, W. G. (1980). General Conservation Equations for Multi-Phase Systems: 3. Constitutive Theory for Porous Media Flow, *Advances in Water Resources* 3: 25–40.

Hassanizadeh, S. M. & Gray, W. G. (1990). Mechanics and Thermodynamics of Multiphase Flow in Porous Media Including Interphase Boundaries, *Advances in Water Resources* 13(4): 169–186.

Hassanizadeh, S. M. & Gray, W. G. (1993a). Thermodynamic Basis of Capillary Pressure in Porous Media, *Water Resources Research* 29(10): 3389 – 3405.

Hassanizadeh, S. M. & Gray, W. G. (1993b). Toward an improved description of the physics of two-phase flow, *Advances in Water Resources* 16(1): 53–67.

Held, R. & Celia, M. (2001). Modeling support of functional relationships between capillary pressure, saturation, interfacial area and common lines, *Advances in Water Resources* 24: 325–343.

Imhoff, P., Jaffe, P. & Pinder, G. (1994). An experimental study of complete dissolution of a nonaqueous phase liquid in saturated porous media, *Water Resources Research* 30(2): 307–320.

IPCC (2005). *Carbon Dioxide Capture and Storage. Special Report of the Intergovernmental Panel on Climate Change*, Cambridge University Press.

Jackson, A., Miller, C. & Gray, W. (2009). Thermodynamically constrained averaging theory approach for modeling flow and transport phenomena in porous medium systems: 6. two-fluid-phase flow, *Advances in Water Resources* 32(6): 779–795.

Joekar-Niasar, V., Hassanizadeh, S. M. & Leijnse, A. (2008). Insights into the relationship among capillary pressure, saturation, interfacial area and relative permeability using pore-scale network modeling, *Transport in Porous Media* 74: 201–219.

Joekar-Niasar, V., Hassanizadeh, S. M., Pyrak-Nolte, L. J. & Berentsen, C. (2009). Simulating drainage and imbition experiments in a high-porosity micro-model using an unstructured pore-network model, *Water Resources Research* 45(W02430, doi:10.1029/2007WR006641).

Kalaydjian, F. (1987). A Macroscopic Description of Multiphase Flow in Porous Media Involving Spacetime Evolution of Fluid/Fluid Interface, *Transport in Porous Media* 2: 537 – 552.

Lüdecke, C. & Lüdecke, D. (2000). *Thermodynamik*, Springer, Berlin.

Marle, C.-M. (1981). From the pore scale to the macroscopic scale: Equations governing multiphase fluid flow through porous media, *Proceedings of Euromech 143*, pp. 57–61. Delft, Verruijt, A. and Barends, F. B. J. (eds.).

Mayer, A. & Hassanizadeh, S. (2005). *Soil and Groundwater Contamination: Nonaqueous Phase Liquids*, American Geophysical Union.

Miller, C., Poirier-McNeill, M. & Mayer, A. (1990). Dissolution of trapped nonaqueous phase liquids: Mass transfer characteristics, *Water Resources Research* 21(2): 77–120.

Niessner, J. & Hassanizadeh, S. (2008). A Model for Two-Phase Flow in Porous Media Including Fluid–Fluid Interfacial Area, *Water Resources Research* . 44, W08439, doi:10.1029/2007WR006721.

Niessner, J. & Hassanizadeh, S. (2009a). Modeling kinetic interphase mass transfer for two-phase flow in porous media including fluid–fluid interfacial area, *Transport in Porous Media* . doi:10.1007/s11242-009-9358-5.

Niessner, J. & Hassanizadeh, S. (2009b). Non-equilibrium interphase heat and mass transfer during two-phase flow in porous media—theoretical considerations and modeling, *Advances in Water Resources* 32: 1756–1766.

Porter, M., Schaap, M. & Wildenschild, D. (2009). Lattice-boltzmann simulations of the capillary pressure-saturation-interfacial area relationship for porous media, *Advances in Water Resources* 32(11): 1632–1640.

Powers, S., Abriola, L. & Weber, W. (1992). An experimental investigation of nonaqueous phase liquid dissolution in saturated subsurface systems: steady state mass transfer rates, *Water Resources Research* 28: 2691–2706.

Powers, S., Abriola, L. & Weber, W. (1994). An experimental investigation of nonaqueous phase liquid dissolution in saturated subsurface systems: transient mass transfer rates, *Water Resources Research* 30(2): 321–332.

Reeves, P. & Celia, M. (1996). A functional relationship between capillary pressure, saturation, and interfacial area as revealed by a pore-scale network model, *Water Resources Research* 32(8): 2345–2358.

Schaefer, C., DiCarlo, D. & Blunt, M. (2000). Experimental measurements of air–water interfacial area during gravity drainage and secondary imbition in porous media, *Water Resources Research* 36: 885–890.

van Antwerp, D., Falta, R. & Gierke, J. (2008). Numerical Simulation of Field-Scale Contaminant Mass Transfer during Air Sparging, *Vadose Zone Journal* 7: 294–304.

Wildenschild, D., Hopmans, J., Vaz, C., Rivers, M. & Rikard, D. (2002). Using X-ray computed tomography in hydrology. Systems, resolutions, and limitations, *Journal of Hydrology* 267: 285–297.

Zhang, H. & Schwartz, F. (2000). Simulating the *in situ* oxidative treatment of chlorinated compounds by potassium permanganate, *Water Resources Research* 36(10): 3031–3042.
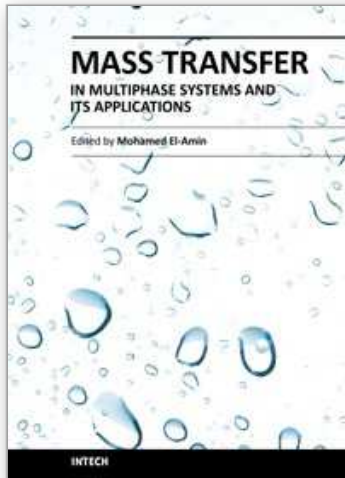
Mass Transfer in Multiphase Systems and its Applications

Edited by Prof. Mohamed El-Amin

ISBN 978-953-307-215-9

Hard cover, 780 pages

Publisher InTech

Published online 11, February, 2011

Published in print edition February, 2011

This book covers a number of developing topics in mass transfer processes in multiphase systems for a variety of applications. The book effectively blends theoretical, numerical, modeling and experimental aspects of mass transfer in multiphase systems that are usually encountered in many research areas such as chemical, reactor, environmental and petroleum engineering. From biological and chemical reactors to paper and wood industry and all the way to thin film, the 31 chapters of this book serve as an important reference for any researcher or engineer working in the field of mass transfer and related topics.

How to reference

In order to correctly reference this scholarly work, feel free to copy and paste the following:

Jennifer Niessner and S. Majid Hassanizadeh (2011). Mass and Heat Transfer During Two-Phase Flow in Porous Media - Theory and Modeling, Mass Transfer in Multiphase Systems and its Applications, Prof. Mohamed El-Amin (Ed.), ISBN: 978-953-307-215-9, InTech, Available from: http://www.intechopen.com/books/mass-transfer-in-multiphase-systems-and-its-applications/mass-and-heat-transfer-during-two-phase-flow-in-porous-media-theory-and-modeling

INTECH
open science | open minds